THE UNIVERSITY OF CHICAGO

FINITE CURVED CREASES IN INFINITE ISOMETRIC SHEETS

A DISSERTATION SUBMITTED TO
THE FACULTY OF THE DIVISION OF THE PHYSICAL SCIENCES
IN CANDIDACY FOR THE DEGREE OF
DOCTOR OF PHILOSOPHY

DEPARTMENT OF PHYSICS

BY
AARON JEREMY MOWITZ

CHICAGO, ILLINOIS
DECEMBER 2020

TABLE OF CONTENTS

LIST OF FIGURES

ACKNOWLEDGMENTS

There are several people I'd like to thank for making my time in graduate school not just a great learning experience, but also a fun and enjoyable one. I'd first like to thank my advisor, Tom Witten. Anybody who knows Tom knows that his joy and passion for everything he does, whether science-related or not, is extremely infectious, and being around that kind of energy has made it a great pleasure working with him. His door is always open, both figuratively and literally, as anyone in the JFI can attest to, and he has always been willing and eager to discuss whatever is on my mind. I've learned and grown a great deal as a scientist and problem-solver from his seemingly boundless knowledge and intuition. As my mentor, he has been encouraging and patient every step of the way, and for that, I couldn't ask for a better advisor. I'd also like to thank the members of my committee: Jiwoong Park, Jon Simon, and Vincenzo Vitelli. Over the past few years they have passed on very valuable wisdom to me as I have progressed through my PhD.

Next, I'd like to thank all of the members of the Witten group I've met over the years: Brian Moths, Anshuman Pal, Lara Braverman, and Tony Song. It's been great getting to know you all and I'm glad I've had the chance to discuss many interesting scientific questions within our group. I'd also like to thank my fellow fish of the fishbowl, aka my office mates: Kabir, Wee, Jackson, Nachi, Vedant, Jiayi, Ryo, and Martin. I've certainly missed our (sometimes wacky) conversations and having your company during these last several months of my PhD, and will definitely miss you all in the future. I also want to thank all of the members of the soft matter groups here at UChicago. I'm glad to have met many of you through IRG meetings, journal clubs, and hanging out in the basement of GCIS, and I'm happy to have been part of such welcoming community.

I'd next like to thank all of the amazing friends I've made during my time in Chicago: Tom, Kieran and Pearl, Gerwin, Mary, Clai and Jungmin, Chris and Lisa, Nathan and Rachel, Patrick, Lisa, Chloe, Lukas, Will, Frank, Samantha, and Andrew. From playing board games, to exploring the city, to playing music, to just simply hanging out and spending

quality time, I'm grateful to have met such wonderful people. I'll certainly cherish all of the memorable moments I've had with you all, and I can't wait to see what the future has in store for all of us!

Finally, I'd like to thank my family: my dad, Ira, my mom, Carol, and my brother, Zachary. They have always supported all of my endeavors, and have always been there for me through all of the highs and lows of graduate school. I would not have made it where I am today without your love and support.

ABSTRACT

Geometric stress focusing, e.g. in a crumpled sheet, creates point-like vertices that terminate in a characteristic local crescent shape. The observed scaling of the size of this crescent is an open question in the stress focusing of elastic thin sheets. According to experiments and simulations, this size depends on the outer dimension of the sheet, but intuition and rudimentary energy balance indicate it should only depend on the sheet thickness. We address this discrepancy by modeling the observed crescent with a more geometric approach, where we treat the crescent as a curved crease in an isometric sheet. Although curved creases have already been studied extensively, the crescent in a crumpled sheet has its own unique features: the material crescent terminates within the material, and the material extent is much larger than the extent of the crescent. These features together with the general constraints of isometry lead to constraints linking the surface profile to the crease-line geometry. We construct several examples obeying these constraints, showing finite curved creases are fully realizable. This approach has some particular advantages over previous analyses, as we are able to describe the entire material without having to resort to excluding the region around the sharp crescent. Finally, we deduce testable relations between the crease and the surrounding sheet, and discuss some of the implications of our approach with regards to the scaling of the crescent size.

CHAPTER 1

INTRODUCTION

Emergent structures are omnipresent in nature. Groups of birds exhibit collective flocking behavior in space and time [2]. Layered fluids of different density form intricate fingering patterns [3]. From spontaneous magnetization [4], to the self-assembly of molecules [5], to shear thickening in colloidal suspensions [6], to the distribution of matter in Saturn's rings [7], these structures can be observed on many different length scales. One can also see similar structures abstractly, such as in non-linear oscillations in dynamical systems [8], and even in the harmonic structure of music [9].

Typically emergent structure leads to a breaking of spatial symmetry. The prototypical instance is crystallization, where collections of atoms or molecules condense and arrange themselves into lattices, resulting in a highly-ordered system that breaks translational symmetry. One sees emergent structure in other phase transitions as well, where the structure will exhibit self-similarity near a critical point.

As one moves to the continuum limit, where elasticity can properly describe the mechanical deformations of a material, more macroscopic structures appear. Biology holds many examples, such as helical coiling of vines [10], ruffles along the edges of lotus leaves [11], and embryonic tissue development [12]. Emergent structures in media may also arise beyond the elastic limit in the realm of irreversible material failure, where the yield stress of material is surpassed. Examples include geological fracture [13], necking in ductile metals [14], and tearing of plastic sheets [15]. These structures arise via some type of forcing, as the material responds by storing elastic energy and changing shape. Different forcing programs will lead to different structures, and a natural question to ask is what forcing is needed to yield a desired structure.

If we consider materials whose extent is small in one or two dimensions, emergent structures are more commonly seen, due to these materials being more easily deformable. These structures are of particular interest because one observes a 3-dimensional structure in an

inherently lower dimensional material. These have led to interesting mathematical theorems about the embedding of low dimensional objects in higher dimensional spaces [16]. The most basic example of emergent structure in a low-dimensional material is the buckling of a 1-dimensional beam, first described by Euler [17]. One applies a compressive force to the beam until a critical load is reached, at which point the straight configuration is no longer stable and the beam curves and buckles. When one moves to 2-dimensional sheets, the same basic buckling behavior can be seen when one applies a load to two opposite sides of the material. However, much richer structures can arise, such as buckling patterns in twisted ribbons under tension [18], azimuthal wrinkling observed in disks suspended on a liquid drop [19], and paper origami which can lead to mechanical metamaterials [20].

An interesting subclass of emergent structures are those where large deformations are localized to small regions of the material. While this phenomenon is very commonplace, it goes against our intuition from thermodynamics. If one injects energy into a system, one expects the energy instead to distribute itself uniformly across the system's size. A paradigmatic example of this localized behavior is seen in fluid boundary layers in pipe flow, where a large amount of viscous drag occurs near the pipe wall [21]. Another example are the caustic networks of reflected light observed in bodies of water [22]. The size of and the amount of energy stored in these localized region often exhibit power-law behaviors in a regime where a system parameter is asymptotically small. These same kinds of power laws are seen in many of the emergent behaviors referred to above.

One particular phenomenon of interest in this subclass is thin-sheet crumpling. If one compresses a thin sheet, such as a piece of paper, along its boundaries, the sheet begins to buckle. However, instead of exhibiting large wavelength deformations, the material develops highly connected networks of vertices and ridges spanning its entire extent. These networks form before the yield stress threshold is reached, but eventually the material plastically deforms, leading to the pattern of creases one sees after unfurling a crumpled piece of paper [23, 24, 25]. Understanding the nature of this stress focusing in thin sheets may provide

some much needed insight on boundary layers in elastic materials. Furthermore, being able to manipulate these networks may prove useful for designing localized structures in materials via particular ways of external forcing.

In this thesis, we propose a new geometric approach of understanding the extent of stress focusing near a vertex in a crumpled sheet. In Chapter 2, we review how stress focusing arises in crumpled sheets. We introduce the prototypical model of a vertex and review previous work on determining the size of the stress focused region around a vertex. In Chapter 3, we introduce our approach. In the prototypical vertex model, one observes a 1-dimensional structure in the shape of a crescent. We argue that this crescent be can described by a separately studied structure known as a curved crease. We outline the geometric constraints which make a curved crease compatible with thin-sheet elasticity. In Chapter 4, we restrict ourselves to creases which more closely resemble the observed crescent. The defining characteristic of this crescent is that it terminates within the material. Furthermore, the extent of the surrounding material is much larger than the size of the material. We derive the geometric constraints which are necessary for a curved crease to exhibit these characteristics. In Chapter 5, we describe several examples of curved creases which obey these constraints. In Chapter 6, we discuss the elastic energy stored in these finite creases, and argue how our approach can avoid the pitfalls of previous approaches. Finally, in Chapter 7, we discuss predictions of our approach that are experimentally testable, and describe future directions and possible limitations our approach has with regard to understanding stress focusing in a crumpling vertex.

CHAPTER 2

STRESS FOCUSING

2.1 Crumpling of thin sheets

As a first step to explain crumpling, we start by considering an initially flat thin sheet, whose thickness h is much smaller than the other dimensions of the material. The deformations of this sheet can then be described by deformations of the midplane, and can be separated into two types: in-plane stretching of the sheet, which leads to strain within the midplane, and out-of-plane bending, which gives rise to curvature of the midplane surface. Each of these deformation modes has an energy cost, which can be found from the 3-dimensional strain induced by each mode [26]. For a homogeneous isotropic sheet with a Young's modulus Y and Poisson ratio ν, the stretching energy E_S is given by

$$E_S = \frac{hY}{2(1-\nu^2)} \int dA \left[\nu (\mathrm{tr}\, \gamma_{ij})^2 + (1-\nu) \mathrm{tr}\, \gamma_{ij}^2 \right] \tag{2.1}$$

where γ_{ij} is the two-dimensional strain tensor of the midplane [26]. Similarly, the bending energy E_B is

$$E_B = \frac{h^3 Y}{24(1-\nu^2)} \int H^2 \, dA \tag{2.2}$$

where H is the mean curvature of the midplane surface, defined as the average of the principal surface curvatures [26]. There is also a term proportional to the integrated Gaussian curvature K, but due to the Gauss-Bonnet theorem, this term does not change with any smooth deformation, and so we need not include it [27].

While it intuitively seems that these two modes are independent, it turns out that the midplane strain and curvature are geometrically constrained. This is due to Gauss' Theorema Egregium, which states that the Gaussian curvature of a surface is invariant under deformations which preserve lengths within the surface [27]. In terms of mechanics, this means that an initially flat sheet will maintain zero Gaussian curvature everywhere if it does

not undergo any stretching, i.e. if γ_{ij} is zero everywhere.

If one compares the stretching and bending energies, specifically their dependence on the sheet thickness, one sees that for a given surface shape, the ratio of bending to stretching energies goes as h^2. This indicates that for thin sheets, it costs more energy to stretch than to bend, so that when $h \to 0$, any amount of stretching is indefinitely costly relative to bending energetically. Such zero-thickness sheets are called isometric, and their equilibrium configurations occur when E_B is a minimum subject to the constraint that γ_{ij} (and therefore E_S) is zero.

We mentioned earlier that a flat sheet that is deformed without stretching will preserve its Gaussian curvature. Since a flat sheet has $K = 0$ everywhere, a deformed isometric sheet must have $K = 0$ everywhere as well. By definition, the Gaussian curvature is the product of the principal surface curvatures, so if K vanishes everywhere, there must be a principal direction of zero curvature at each point in the material. These directions are known as generators, and a surface described by these generators is known as a developable surface [27].

Due to the requirement of unstretchability, there are strong constraints on the extent to which one can uniformly confine an isometric sheet. If one tries to uniformly confine the sheet to a region smaller than the size of the sheet R, in order to avoid bending of generators, the sheet develops "vertices" where generators meet at a point within the material. Due to this converging of directions, the shape of the material around such a vertex will be cone-like. As one confines the sheet further, more vertices appear, maintaining unstretchability. When the sheet has been confined enough so that two of these vertices are within the vicinity of one another, the generators emanating from these vertices will begin to overlap within the material. If one considers a point in the material where this overlap occurs, one has two independent directions of zero curvature. This means these regions of overlap must be completely flat. The one exception is the line that joins the two vertices. The material will fold along this line, giving rise to a sharp straight crease, or "ridge." So besides the conical

regions where material generators meet at a vertex, the sheet is flat everywhere except near vertices and ridges, and almost all of the elastic stress is localized at these singular structures, due to the large bending deformations in these regions. As the sheet continues to be confined, networks of these vertices joined by ridges develop, leading to the structures one commonly sees in a crumpled sheet of paper.

A real finite-thickness sheet will also exhibit vertices and ridges, but these regions will be accompanied by some amount of stretching. If the sheet were truly unstretchable, it would cost an infinite amount of bending energy to form vertices and ridges, due to their sharp nature. Allowing for stretching relaxes this divergence. Furthermore, a natural length scale must emerge from the balance between bending and stretching, determining the size of the regions where stress is localized. This has been thoroughly studied for a stretching ridge, where the width has been shown to scale as $h^{1/3}R^{2/3}$ [28]. However, the scaling of stress focusing in a vertex has proven to be much more subtle issue, as we shall now see.

2.2 D-cone core scaling

As with ridges, the size of the region around a vertex where stretching occurs will be finite. There is a straightforward way to study a single vertex in isolation: if one takes a thin sheet and pushes it into a circular ring, one gets a structure known as a developable cone, or d-cone for short [29]. In the zero-thickness limit, the material is unstretched everywhere except at the central forcing point, and has straight generators emanating from this point (hence the name developable). Due to its conical shape and the confining nature of the forcing, the d-cone serves as a paradigm for studying vertices in crumpled sheets, and has been studied extensively both via experiments and simulations [30, 31, 32, 33, 34, 35].

The bending energy of a d-cone can be calculated from the curvature. Due to the locally conical geometry, the curvature goes as $1/r$, where r is the distance from the forcing point, and therefore has a divergence at the center. In order to maintain a finite energy, some distortion from this ideal cone structure is necessary, at least within some small region of

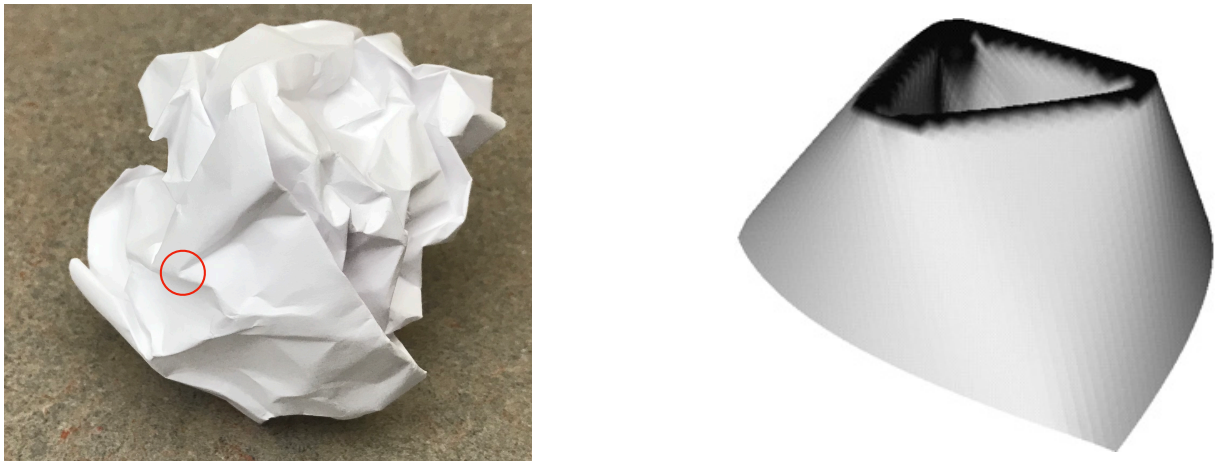

Figure 2.1: Curved crescents in thin sheets. Left shows a crescent observed at the vertex of a crumpled sheet, circled in red. Right shows crescents seen at the corners of a buckled ring ridge (reproduced from [1]).

size R_c. Supposing no appreciable distortion for $r > R_c$, one can then find the scaling of the bending energy:

$$E_B \sim h^3 Y \int_{R_c}^{R} \frac{1}{r^2} r\, dr \sim h^3 Y \log \frac{R}{R_c}. \tag{2.3}$$

One typically treats R_c as a cutoff radius, separating the outside conical region from the inner region, which is referred to as the d-cone core. In a real finite-thickness sheet, the material will exhibit stretching, which one presumes to be localized to the core region, similar to the vertex in a crumpled sheet. As in the stretching ridge, there will be competition between stretching and bending, leading to stress focusing in the core. This physically manifests itself in the material as a sharp crescent whose length is commonly taken as a measure of R_c [30]. These crescents are seen in crumpled sheets, as well as at the corners of a buckled ring ridge, as seen in Fig. 2.1. Because this region is completely localized around the tip, one would expect its size should not depend on any outer dimensions of the sheet, i.e. the size of the sheet R or the size of the confining ring R_p. It is therefore expected that $R_c \sim h$, which is supported by a more rigorous energy-balance argument [32].

If one removes a disk of radius R_c from the center of a flat sheet and pushes it into a confining ring, the resulting shape will be that of a d-cone with its tip removed, whose energy

cost is given by Eq. (2.3). This energy alone prefers a large R_c, since it will be smaller for larger R_c, and its derivative with respect to R_c is independent of R. In order for there to an optimal finite R_c, there must be an additional contribution to the total energy that prefers small R_c. If one now re-attaches the disk to the inner boundary of the truncated d-cone, the disk must deform in order to close the surface and will therefore cost elastic energy. The distortion of the disk may, for example, be similar to that of spherical cap, and so will exhibit a mean curvature of order $1/R_c$. This means that the energy cost due to bending will be of order $h^3 Y (1/R_c)^2 R_c^2 \sim R_c^0$, i.e. it will be independent of R_c. The distorted disk will also exhibit Gaussian curvature of order $1/R_c^2$, and so will have a stretching energy cost of order hYR_c^2. This energy prefers small R_c, and so competes with the energy of the outer region. However, it is independent of R, so that if one minimizes the sum of the bending energy of the outer region and the stretching energy of the inner disk, the result is $R_c \sim h$.

The above argument indicates that the core radius should be independent of the outer dimension of the sheet. However, both simulations and experiments have measured an R_c which does depend on the sheet size, and appears to vary as $h^{1/3}R^{2/3}$, the same as a stretching ridge. Furthermore, Cerda and Mahadevan [30] have proposed a different energy-balance argument that includes stretching due to having a finite-size core, which lengthens the radial generators. This analysis leads to the observed scaling of R_c that depends on R.

While it appears the core size scaling is fully explained by this argument, there are still some inconsistencies. The stretching due to lengthening of generators that Cerda and Mahadevan include in their analysis would normally be present in the d-cone outer region in addition to the core. This stretching would have an unphysically large energy cost and would completely dominate the already present bending energy from Eq. (2.3). It may be possible that the stretching is completely localized to the core region, but no argument has been put forth to justify this [24]. Furthermore, the d-cone simulations and experiments are limited by the range of sheet thickness they can probe, and typically only use a single order of magnitude range of h when measuring R_c. Thus there is still an explanation to be found

for the observed scaling of R_c. Still, for the moment it appears that the core size increases indefinitely with R for fixed h and decreases indefinitely with h at fixed R.

CHAPTER 3

CURVED CREASES

3.1 D-cone crescent as a curved crease

We turn back to the observed crescent in the d-cone core. The stretching in the core region occupies a finite area around the crescent. If we take the limit as $h \to 0$, the crescent will shrink to a point, where the stretching will be localized, just like in a real cone. However, if R_c does have a power law dependence on R, we may at the same time take the limit as $R \to \infty$ in such a way that R_c is kept fixed as $h \to 0$. In this case, we maintain a crescent of finite size, where the stretching is now localized to the crescent line, so that the material is isometric everywhere else. What we are therefore left with is a sharp curved crease in an isometric sheet. This provides a new way to study the d-cone core region, as we shall see.

Curved creases have been a topic of interest in the field of thin elastic sheets for several decades. If one draws a curved line on a flat piece of paper and folds along that line, the material develops 3-dimensional structure. The curve is no longer planar and the surfaces on either side become curved in a way such that they are compatible with the curvature of the crease line, which is determined by the shape of the planar curve and the opening angle of the fold. These creases have been studied by computer scientists [36] and engineers [37] as an avenue for designing new geometric shapes. More recently, there has been an interest in curved creases made out of real finite-thickness materials. A simple example is the buckled structure that is formed when one folds along the midline of a circular annulus [38, 39, 40], due to geometric frustration from having a closed curve. The d-cone crescent seems to be a likely candidate as a curved crease, but there are two key differences that separate it from previously studied cases. The crescent is in a sheet of large extent, and the crescent line terminates within the material. There have been studies attempting to model the d-cone that account for either one of these features [41, 42, 43], but as of yet, no one has explicitly laid out geometric constraints that yield both of these characteristics. We will do just that,

but we first present the background necessary to describe curved creases in isometric sheets.

3.2 Geometry of curves and surfaces

We first remind ourselves of some fundamental notions from geometry of curves and surfaces. Much of this is covered in standard references on differential geometry [27, 44], but we will present these ideas in the context of curved creases, following the conventions used in [37] and [38]. We start with a space curve $\vec{X}(s)$ parametrized by arc-length. We define the tangent vector field $\hat{t}(s)$ of $\vec{X}(s)$ as the derivative of $\vec{X}(s)$ with respect to arc-length: $\hat{t}(s) \equiv \vec{X}'(s)$. Since $\vec{X}(s)$ is parametrized by arc-length, and is therefore unit-speed, $\hat{t}(s)$ must be a unit vector. We can then define a second vector field $\hat{n}(s)$ as the normalized derivative of the tangent: $\hat{n}(s) \equiv \hat{t}'(s)/\|\hat{t}'(s)\|$. This is known as the curve normal vector field, and must be orthogonal to $\hat{t}(s)$, since $\hat{t}(s)$ is a unit vector. We finally define the binormal vector field $\hat{b}(s)$ as the cross product between the tangent and normal vector fields: $\hat{b}(s) \equiv \hat{t}(s) \times \hat{n}(s)$. We therefore now have an orthonormal frame defined at each point along the curve, $\{\hat{t}(s), \hat{n}(s), \hat{b}(s)\}$, known as the Frenet-Serret frame:

$$\hat{t}(s) \equiv \vec{X}'(s) \tag{3.1a}$$

$$\hat{n}(s) \equiv \hat{t}'(s)/\|\hat{t}'(s)\| \tag{3.1b}$$

$$\hat{b}(s) \equiv \hat{t}(s) \times \hat{n}(s). \tag{3.1c}$$

Fig. 3.1 shows an example of this frame for a given curve.

The Frenet-Serret frame allows one to define the intrinsic shape of the curve using two scalar functions, a curvature denoted $\kappa(s)$ and a "torsion" denoted by $\tau(s)$. These scalars

are defined by what are known as the Frenet-Serret formulas [27]:

$$\hat{t}'(s) = \kappa(s)\hat{n}(s) \tag{3.2a}$$

$$\hat{n}'(s) = -\kappa(s)\hat{t}(s) + \tau(s)\hat{b}(s) \tag{3.2b}$$

$$\hat{b}'(s) = -\tau(s)\hat{n}(s). \tag{3.2c}$$

The curvature, which is simply the magnitude of $\hat{t}'(s)$, tells one how much a curve deviates from a linear trajectory, and is non-negative. In mechanical terms, if $\vec{X}(s)$ represents the trajectory of a moving particle, $\kappa(s)$ is the magnitude of the particle's normal acceleration. Often $\hat{t}'(s)$ is referred to as the vector curvature $\vec{\kappa}(s)$, and always points in the direction in which $\vec{X}(s)$ is curving. The torsion measures how much the curve is twisting out the plane spanned by $\hat{t}(s)$ and $\hat{n}(s)$ (known as the plane of curvature), and so tells how non-planar $\vec{X}(s)$ is. The sign of $\tau(s)$ is a matter of convention, but here is chosen so that a right-handed helix has positive torsion. The curvature and torsion completely determine $\vec{X}(s)$ up to rigid-body motions, as one can integrate Eq. (3.2) to find the Frenet-Serret frame, in particular the tangent $\hat{t}(s)$, and then integrate Eq. (3.1a) to find $\vec{X}(s)$.

The Frenet-Serret frame is useful for completely characterizing a curve in space. However, if we have a curve that lies on a curved surface, it is useful to have an orthonormal frame that relates the curvature and torsion of the curve to the curvature of the surface. We now consider a curve $\vec{X}(s)$ (again parametrized by arc-length) on an arbitrary surface S, and start with the curve tangent $\hat{t}(s)$ as the first vector field of our orthonormal basis. If our surface is orientable and we have chosen a particular orientation, S has a well-defined smooth unit normal vector field $\hat{N}_S$ which is orthogonal to the tangent plane at each point on S. In particular, at each point along $\vec{X}(s)$, $\hat{t}$ and $\hat{N}_S$ will be orthogonal to guarantee that the curve lies in the surface. Therefore, if along our curve we define $\hat{N}(s) \equiv \hat{N}_S(\vec{X}(s))$, we have a second orthonormal vector field, which we will call the surface normal vector field. To complete our basis, we define a third vector field $\hat{u}(s)$, known as the normal tangent

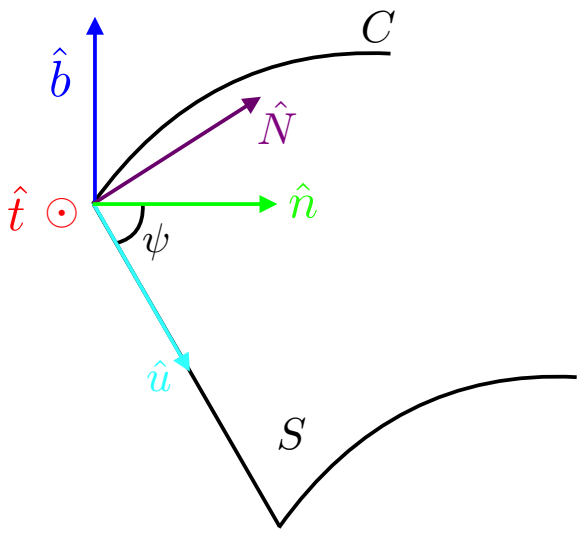

Figure 3.1: Co-ordinate bases for curves within surfaces. The curve marked C is directed out of the page at one point, and is bending to the right. The Frenet-Serret basis ($\hat{t}$, $\hat{n}$, $\hat{b}$) of Eq. 3.1 is shown at this point. The embedding surface is marked S with its surface normal $\hat{N}$. The Darboux basis ($\hat{t}$, $\hat{u}$, $\hat{N}$) of Eq. 3.3 is shown. ψ is the angle between the two bases, demonstrating they are related by a rotation about the curve tangent $\hat{t}$.

vector field, as the cross product between the surface normal and tangent vector fields: $\hat{u}(s) \equiv \hat{N}(s) \times \hat{t}(s)$. $\hat{u}(s)$ is then a vector tangent to S and and perpendicular to the curve tangent. Evidently $\hat{t}(s)$ and $\hat{u}(s)$ then form a basis tangent to the surface at s. Combined with the surface normal, we therefore have an orthonormal frame defined along our curve, $\{\hat{t}(s), \hat{u}(s), \hat{N}(s)\}$, which is known as the Darboux frame [44]:

$$\hat{t}(s) \equiv \vec{X}'(s) \tag{3.3a}$$

$$\hat{N}(s) \equiv \hat{N}_S(\vec{X}(s)) \tag{3.3b}$$

$$\hat{u}(s) \equiv \hat{N}(s) \times \hat{t}(s). \tag{3.3c}$$

Since both the Frenet-Serret and Darboux frames share the common vector $\hat{t}(s)$, they are

related by a rotation about $\hat{t}(s)$:

$$\hat{n}(s) = \cos\psi(s)\,\hat{u}(s) + \sin\psi(s)\,\hat{N}(s) \tag{3.4a}$$

$$\hat{b}(s) = -\sin\psi(s)\,\hat{u}(s) + \cos\psi(s)\,\hat{N}(s) \tag{3.4b}$$

where ψ is the angle between $\hat{n}(s)$ and $\hat{u}(s)$. Fig. 3.1 shows an example of the Darboux frame for a curve lying on a surface.

Similar to the Frenet-Serret case, one can define three scalar quantities $\kappa_g(s)$, $\kappa_N(s)$, and $\tau_g(s)$ from the rate-of-change of the Darboux frame:

$$\hat{t}'(s) = \kappa_g(s)\hat{u}(s) + \kappa_N(s)\hat{N}(s) \tag{3.5a}$$

$$\hat{u}'(s) = -\kappa_g(s)\hat{t}(s) + \tau_g(s)\hat{N}(s) \tag{3.5b}$$

$$\hat{N}'(s) = -\kappa_N(s)\hat{t}(s) - \tau_g(s)\hat{u}(s). \tag{3.5c}$$

$\kappa_g(s)$ and $\kappa_N(s)$ are known as the geodesic and normal curvatures, respectively, and are the components of $\vec{\kappa}(s)$ tangent and normal to S ($\kappa_g(s)\hat{u}(s)$ and $\kappa_N(s)\hat{N}(s)$ are sometimes written as $\vec{\kappa}_g(s)$ and $\vec{\kappa}_N(s)$, so that $\vec{\kappa}(s) = \vec{\kappa}_g(s) + \vec{\kappa}_N(s)$). $\tau_g(s)$ is known as the geodesic torsion, and measures how much the curve is twisting out of the surface tangent plane.

It is worth mentioning that the Frenet-Serret scalars, $\kappa(s)$ and $\tau(s)$, and the Darboux scalars, $\kappa_g(s)$, $\kappa_N(s)$, and $\tau_g(s)$, can be related to each other. If we combine Eqs. (3.2a) and (3.5a), replace $\hat{n}(s)$ with Eq. (3.4a), and equate the coefficients of $\hat{u}(s)$ and $\hat{N}(s)$ on either side, we get

$$\kappa_g(s) = \kappa(s)\cos\psi(s) \tag{3.6a}$$

$$\kappa_N(s) = \kappa(s)\sin\psi(s), \tag{3.6b}$$

which is just another statement of $\kappa_g(s)$ and $\kappa_N(s)$ being independent components of $\vec{\kappa}(s)$. From Eq. (3.5b), we see that $\tau_g(s) = \hat{u}'(s)\cdot\hat{N}(s)$. If we invert Eqs. (3.4) to express $\hat{u}(s)$

and $\hat{N}(s)$ in terms of $\hat{n}(s)$ and $\hat{b}(s)$, and differentiate the expression for $\hat{u}(s)$ (making use of Eqs. (3.2)), we can evaluate this dot product:

$$\tau_g(s) = \tau(s) - \psi'(s). \tag{3.7}$$

This expresses the fact that the rotation of the Darboux frame about $\hat{t}(s)$ can be decomposed into the rotation of the Frenet-Serret frame about $\hat{t}(s)$ (i.e. $\tau(s)$) and the rotation the Darboux frame relative to the Frenet-Serret frame (i.e. $\psi'(s)$).

One last thing to consider is what happens when one deforms a surface with a curve on it. If we require that the curve remain on the surface as the surface is deformed, for a general deformation, its curvature and torsion will change, and the curve is free to move around within the surface. However, if the deformation preserves lengths within the surface (i.e. is isometric), the curve can still change in space, but it must now be fixed within surface. This means its geodesic curvature, the in-plane component of the curvature vector, must remain the same after the deformation. This will be important when we outline the conditions for having a crease in an isometric sheet.

What we have described so far applies to arbitrary smooth surfaces. We now restrict ourselves to flat Euclidean sheets (we also take our sheet to be narrow in one dimension, for reasons that will become clear later). If one draws a curve on a flat asymptotically thin sheet and folds through an opening angle $\theta(s)$ along this curve (see Fig. 3.2), one gets a 3-dimensional structure known as a curved crease. This structure can be thought of as two surfaces meeting a common space curve $\vec{X}(s)$ (again parametrized by arc-length), and since it is formed by an isometric deformation of a flat surface, the two surfaces must be developable. Therefore each surface has a generator at every point, and can be described by the standard parametrization for ruled surfaces:

$$\vec{X}_{\pm}(s, v) = \vec{X}(s) + v\hat{g}_{\pm}(s) \tag{3.8}$$

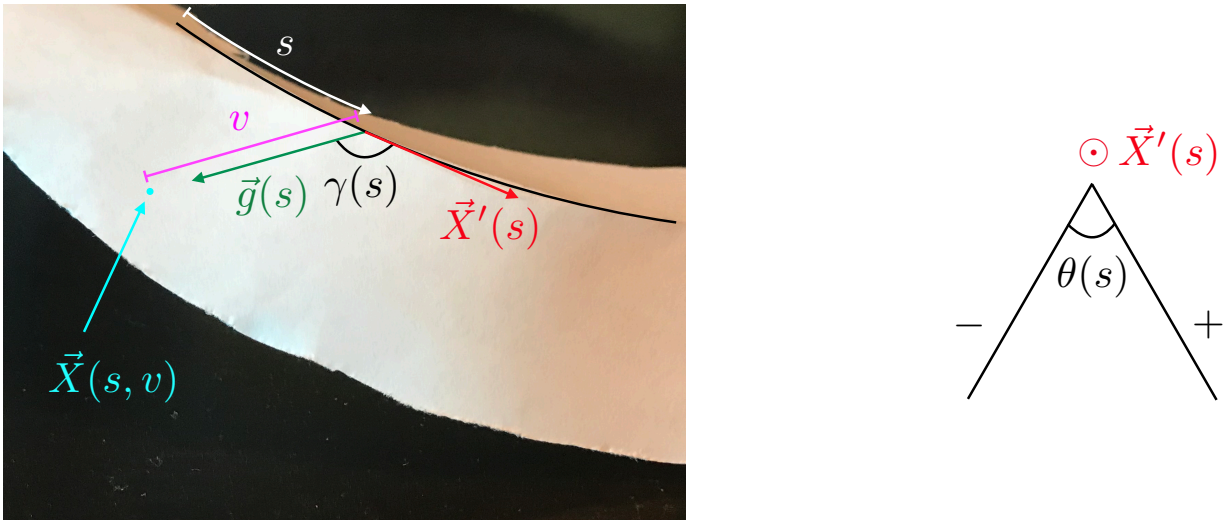

Figure 3.2: Diagrams labeling quantities pertaining to curved crease. The left shows a view of a narrow curved crease whose crease line is indicated by the black line. The right shows a view facing the crease line tangent and indicates the opening angle θ.

where s is the arc-length coordinate, $\hat{g}_{\pm}(s)$ is the direction of a generator at s , and v is the coordinate along generators[1]. $+$ and $-$ are used to distinguish between the two sides of the crease, though we will refer to them here as "inner" and "outer" respectively. Though $\vec{X}_{\pm}(s,v)$ completely describes the crease, one can more easily describe it using the curvature $\kappa(s)$ and torsion $\tau(s)$ of the crease curve, the opening angle of the crease $\theta(s)$, and the angle between the generator and the crease curve tangent, $\gamma_{\pm}(s)$ (see Fig. 3.2). As we will now see, all of these quantities are related due to constraints imposed by having an isometric sheet.

3.3 Constraints due to isometricity

So far, although we have been able to adequately describe a curved crease, we have not imposed any constraints due to the crease being formed by an isometric deformation of a flat sheet. Before one folds along the crease line, the crease curve is planar (i.e. has no torsion),

1. The letter g used to define a generator has no relation to the "geodesic" subscript g used earlier in Section 3.2 for curvatures and torsions

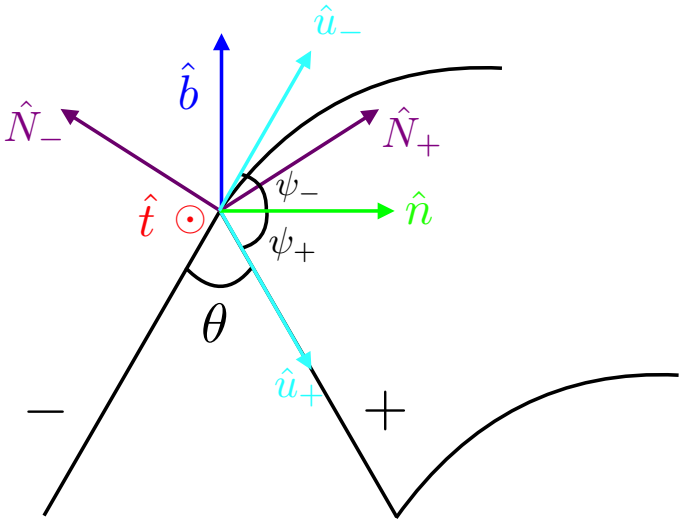

Figure 3.3: Cross section of a crease, indicating the Frenet-Serret and Darboux frames. θ is the opening angle, and $\psi_\pm$ are the angles between $\hat{n}$ and $\hat{u}_\pm$.

and only has geodesic curvature. Once one has made the fold, the crease curve may develop torsion, and will have both normal and geodesic curvature when seen as a curve in either the inner or outer surface. However, as mentioned before, the geodesic curvature does not change under isometric deformations, so the geodesic curvature as measured in the inner surface (κ_{g+}) must equal that measured in the outer surface (κ_{g-}), and must be the same as the curvature of the originally drawn crease line.

Fig. 3.3 shows a segment of the crease at a point s, viewed along the tangent $\hat{t}$, with the normal $\hat{n}$ and binormal $\hat{b}$ to the curve oriented horizontally and vertically. The adjacent "inner" surface on the $\hat{n}$ side of the curve is designated $+$. If this surface were horizontal, its normal tangent vector $\hat{u}_+$ would coincide with $\hat{n}$. This surface is instead rotated clockwise by an angle ψ_+. Thus κ_{g+}, the component of $\vec{\kappa}$ tangent to the inner surface, is given by $\kappa_{g+} = \kappa \cos\psi_+$. This same relation must hold for the outer surface. Since κ and κ_g are the same for both surfaces, the angle ψ_- must have the same cosine as ψ_+. Therefore the two angles must be equal in magnitude; they either coincide or have equal and opposite ψ, and so the angle between the two surface normals, i.e. the angle between $\hat{N}_+$ and $\hat{N}_-$, must be 2ψ. The supplementary opening angle θ between the two surfaces is evidently $\pi - 2\psi$. The

normal components of $\vec{\kappa}$, denoted κ_{N+} and κ_{N-} are likewise given by $\kappa_{N\pm} = \pm\kappa \sin\psi_{\pm}$. We note that this local constraint is independent of any twist in the Frenet-Serret or the Darboux frames. The constraint of equal κ_g thus fixes the relation between the opening angle and the angle ψ between the the two frames at every point s. We refer to this as the "compatibility constraint."

Using this relation, we may straightforwardly rewrite Eq. (3.6) in terms of the opening angle θ. Since 2θ is the supplement of ψ, $\theta' = -\psi'$. Thus for an isometric crease, Eqs. (3.6) and (3.7) become [38]

$$\kappa_g(s) = \kappa(s) \sin\theta(s)/2 \tag{3.9a}$$

$$\kappa_{N\pm}(s) = \pm\kappa(s) \cos\theta(s)/2 \tag{3.9b}$$

$$\tau_{g\pm}(s) = \tau(s) \pm \theta'(s)/2. \tag{3.9c}$$

We mentioned earlier that the surfaces on either side must be developable. Even though it is a well-known fact that developable surfaces are ruled [44], the parametrization given by Eq. (3.8) does not guarantee developability. In order to do so, the directions in which $\hat{g}_{\pm}(s)$ point must be constrained so that they lie along generators in the surface. This constraint leads to a relationship between the crease line tangent $\hat{t}(s)$ and $\hat{g}_{\pm}(s)$: $\vec{t}(s)$, $\hat{g}_{\pm}(s)$, and $\hat{g}'_{\pm}(s)$ must be coplanar [44]. Since $\vec{t}(s)$ and $\hat{g}_{\pm}(s)$ are both tangent to the crease surface, this means that $\hat{g}'_{\pm}(s)$ cannot have a component normal to surface. We can express this requirement in terms of scalar quantities by first writing $\hat{g}_{\pm}(s)$ in terms of the Darboux basis:

$$\hat{g}_{\pm}(s) = \cos\gamma_{\pm}\, \hat{t} \pm \sin\gamma_{\pm}\, \hat{u}_{\pm} \tag{3.10}$$

where $\gamma_{\pm}$ are the generator angles as defined earlier and shown in Fig. 3.2. We then can take the derivative of Eq. (3.10) and use Eqs. (3.5) to express the result purely in terms of

the Darboux basis:

$$\hat{g}'_{\pm}(s) = \mp(\kappa_g \pm \gamma'_{\pm}) \sin\gamma_{\pm}\, \hat{t} + (\kappa_g \pm \gamma'_{\pm}) \cos\gamma_{\pm}\, \hat{u}_{\pm} + (\kappa_{N\pm} \cos\gamma_{\pm} \pm \tau_{g_{\pm}} \sin\gamma_{\pm})\, \hat{N}_{\pm}. \quad (3.11)$$

Setting the normal component of the above to zero and using Eq. (3.9) yields [38]

$$\tan\gamma_{\pm}(s) = -\frac{\kappa(s)\cos\theta(s)/2}{\tau(s) \pm \theta'(s)/2} \quad (3.12)$$

which is our second constraint. We call this the "developability constraint."

It is helpful to have some intuition on how these constraints connect the geometry of the crease curve to that of the surfaces. First, one can see in Fig. 3.3 that as a consequence of compatibility constraint, the binormal vector of the curve must bisect the opening angle of the crease. This means that when one forms a crease with a particular opening angle, the direction of the curvature vector of the crease curve is determined.

Second, consider a crease whose crease curve is a finite arc of a circle, so that it has constant curvature and zero torsion, and a constant opening angle. If one increases or decreases θ, in order to keep κ_g the same, the curvature of the crease curve must increase or decrease (one can see this experimentally by taking a creased ribbon with constant curvature and pinching the two sides: as one pinches, the crease curves further inward). This also excludes the possibility of having an opening angle equal to zero, as then the crease curve will have a diverging curvature.

Finally, we consider the effect of torsion. Taking again the finite arc crease with a constant θ and zero τ, one sees from Eq. (3.12) that $\gamma_{\pm}$ must be 90 degrees, so that if one draws the generators on the surfaces and then flattens the crease, the generators will everywhere be orthogonal to the crease curve (see Fig. 3.4a). If now the horizontal finite arc crease is fixed on one end and lifted on the other, so that it is part of a right-handed helix (and therefore has positive torsion), Eq. (3.12) now tells us that $\gamma_{\pm}$ must be greater than 90

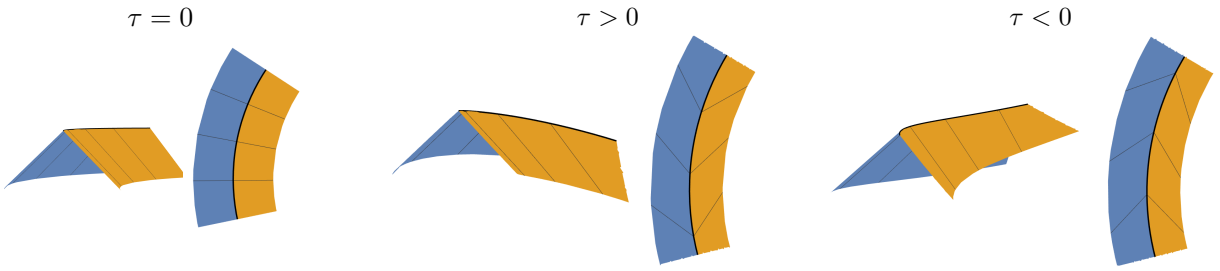

Figure 3.4: Examples of curved creases with different torsions. Curved bold lines indicate the crease curve, orange and blue surfaces correspond to the inner and outer surfaces respectively, and thin straight lines indicate the drawn-on generators. The left picture of each pair is viewed along the crease line tangent, while the right picture is viewed from above the material after the crease has been flattened.

degrees. If one draws the generators and flattens, when viewed from above the "roof" of the crease, the generators will now form chevrons pointing counterclockwise, as seen in Fig. 3.4b. For a left-handed helix ($\tau < 0$), the generators will form chevrons pointing in the opposite direction, as in Fig. 3.4c. We should note that these chevrons will be symmetric about the crease line when the opening angle is constant, since Eq. (3.12) says $\gamma_+ = \gamma_-$ in this case. If one has a varying opening angle, the chevrons will no longer be symmetric (in the case of zero torsion, γ_+ and γ_- will be supplementary angles so that the generators in the flat state will no longer "refract" as they cross the crease line).

With the constraints due to having an isometric crease now fully laid out, it is helpful to know how many and what quantities need to be specified in order to completely determine the shape of a crease. Intuitively, if one folds along line with a given curvature profile, and the opening angle is prescribed a certain profile everywhere along the fold line, it seems the entire shape of crease should be determined. This is true if one also considers the elastic energy of the crease, but the geometric constraints alone are not enough. We can see this by counting the number of quantities needed to describe the crease, and comparing it to the number of constraints.

The shape of the crease line $\vec{X}(s)$ is fully specified by its curvature $\kappa(s)$ and torsion $\tau(s)$, as noted in Section 3.2. The outer and inner surfaces are defined by their generators, whose

directions in space are specified by the generator angles $\gamma_{\pm}(s)$ and the opening angle $\theta(s)$. Finally, one most know the curvature of the crease line within either surface, i.e. the geodesic curvature $\kappa_g(s)$. We therefore have a total of six quantities to be specified. However, this number will be reduced by the isometric constraints. The compatibility constraint will reduce the number by one, as it is a single constraint relating the orientation of the crease line and the opening angle. The developability constraint is a single constraint on each surface that requires them to be developable, and so reduces the number further by two. One therefore needs to specify three quantities of the original six to determine the shape of an isometric crease.

For example, suppose one specifies κ_g, τ, and θ. Eq. (3.9a) will then determine κ, so that the crease line can be found, and Eq. (3.12) will yield the generator angles, so that the generators on both sides will be known. If the condition of minimum energy is also included, then this reduces the number of necessary quantities further by one, which is then consistent with the expectation mentioned above.

As an alternative approach, one could start by specifying the surface on, say, the inner side, assuming it is developable. If one constrains a curve with a particular geodesic curvature profile to lie on this surface, its curvature and torsion will be determined. Furthermore, the generator angle on the inner surface will also be known without reference to the other side of the crease. These three quantities are then sufficient to specify the crease. First, θ may be found from Eq. (3.9a). Then Eq. (3.12) can give the generator angle on the outer surface. These two procedures will be useful when constructing particular examples of curved creases in Chapter 5.

As noted in Section 2.1, the energy content of isometric surfaces, such as those on either side of a crease, depends on their mean curvature $H(s, v)$, as shown by Eq. (2.2). If one considers a generator at s and its neighboring generator, the surface between these two generators will be the section of a cone, whose vertex will be the intersection point of the generators, as shown in Fig. 3.5. Since the mean curvature of a cone at a given

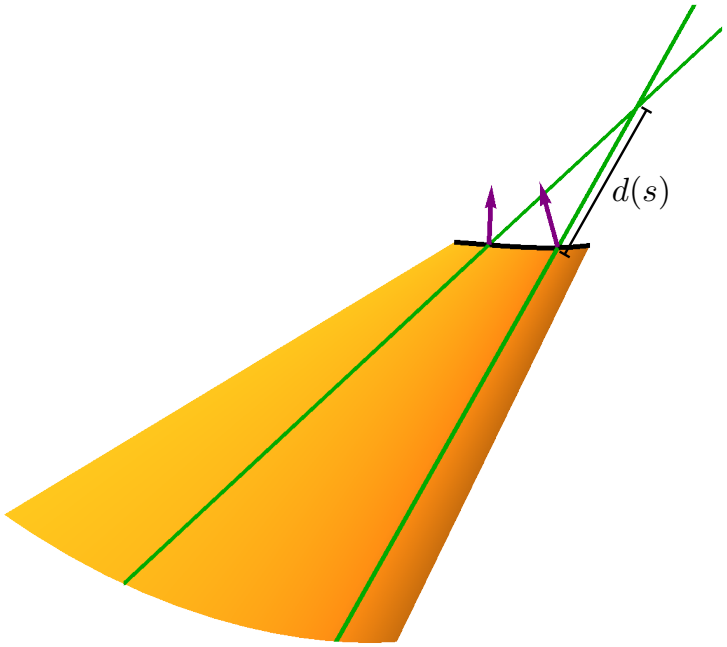

Figure 3.5: Section of a curved crease. Generators are indicated by green lines, the boundary curve is indicated in black, and purple arrows indicate the surface normal along the crease line. Locally the geometry of a curved crease surface is that of a cone, as neighboring generators intersect each other at a point a distance d from the crease line. Thus one can determine the mean curvature at any point in the surface along a generator using d and the mean curvature at the crease line, which is related to the crease line's normal curvature.

point is inversely proportional to the distance from the point to the cone's vertex, the mean curvature of the surface at the coordinates (s, v) will be inversely proportional to $d(s) + v$, where $d(s)$ is the distance on the surface from the crease point s to the intersection point. One can calculate $d(s)$ for both the inner and outer surfaces using planar geometry: $d_{\pm}(s) = \mp \sin \gamma_{\pm}(s)/(\kappa_g(s) \pm \gamma'_{\pm}(s))$.

In order to find the exact expression for $H(s, v)$, we can calculate the mean curvature at a given v, such as the crease line, where $v = 0$. The mean curvature then takes the form $H(s, v) = H(s, 0)/(1 + v/d(s))$. To determine $H(s, 0)$, we may use Euler's theorem, which for a chosen direction, expresses the surface normal curvature κ_N in terms of the principal curvatures κ_0, κ_1 and the angle between our chosen direction and a principal one η [44]: $\kappa_N = \kappa_0 \cos^2 \eta + \kappa_1 \sin^2 \eta$. If we choose the direction to be the crease line tangent, then κ_N is the normal curvature of the crease line, and if we choose the κ_0 direction to be the

generator at s, then κ_0 is zero and η is the generator angle $\gamma(s)$. So the mean curvature at the crease line is $H(s,0) = \kappa_1(s)/2 = (\kappa_N(s)\csc^2\gamma(s))/2$. We can then generalize to both surfaces of our crease, and find the mean curvature at a general point in either surface:

$$H_\pm(s,v) = \frac{\kappa_{N\pm}(s)\csc\gamma_\pm(s)}{2(\sin\gamma_\pm(s) \mp v(\kappa_g(s) \pm \gamma'_\pm(s)))}. \tag{3.13}$$

We note that in the orientation of Fig. 3.3, $H(s,v)$ is necessarily positive (concave) on the inner surface and negative (convex) on the outer one.

We can now determine the bending energy of a curved crease using Eq. (2.2). For our parametrization $\vec{X}_\pm(s,v)$, the area element dA can be written as $\|\partial_s\vec{X}_\pm \times \partial_v\vec{X}_\pm\|\,ds\,dv$ [27]. Then the amount of bending energy stored in the sector of the sheet from a segment of the crease of length ds is given by

$$dE = \frac{B}{2}\,ds \sum_\pm \int H_\pm^2(s,v)\,\|\partial_s\vec{X}_\pm \times \partial_v\vec{X}_\pm\|\,dv, \tag{3.14}$$

where $B \equiv h^3Y/(12(1-\nu^2))$ is the bending stiffness. Calculating $\|\partial_s\vec{X}_\pm \times \partial_v\vec{X}_\pm\|$ and using our expression for $H_\pm(s,v)$ yields

$$dE = \frac{B}{2}\,ds \sum_\pm \int \frac{(\tau \pm \theta'/2)^2\sec^2\gamma_\pm}{4(\sin\gamma_\pm \mp v(\kappa_g \pm \gamma'_\pm))}\,dv. \tag{3.15}$$

The integrand has the form $A/(B+vC)$, where A, B, and C are independent of v. Thus the dv integral from 0 to R is $(A/C)\log((B+RC)/B+RC)$:

$$dE = \frac{B}{8}\,ds \sum_\pm \mp\frac{(\tau \pm \theta'/2)^2\sec^2\gamma_\pm}{\kappa_g \pm \gamma'_\pm}\log\left(\frac{\sin\gamma_\pm \mp R(\kappa_g \pm \gamma'_\pm)}{\sin\gamma_\pm}\right). \tag{3.16}$$

CHAPTER 4

FINITE CURVED CREASES IN SHEETS OF INFINITE EXTENT

4.1 Additional constraints

The discussion in the previous section considered creases in arbitrarily narrow strips. Our aim is to study creases in an infinite sheet. The requirement that this infinite region be isometric imposes additional constraints on the crease itself. Although a set of generators defined along the crease curve give a well-defined surface, this does not preclude the possibility of nearby generators intersecting each other, which would lead to singularities in the sheet. If we consider narrow sheets as we did above, this is not an issue, as we can take our sheet to be narrow enough so that neighboring generators do not have the chance to cross. However, if we consider infinitely large sheets, we must impose a condition that prevents intersecting generators. In order to do this, let us consider two neighboring generators in the inner surface along $\hat{g}_+(s)$ and $\hat{g}_+(s+ds)$, as shown in Fig. 4.1. As one moves along the crease line from s to $s+ds$, $\hat{g}_+(s)$ will rotate in space to form an angle $d\omega$ with $\hat{g}_+(s+ds)$. To avoid the line along $\hat{g}_+(s+ds)$ intersecting with the the line along $\hat{g}_+(s)$, the rotation must be clockwise, so that $d\omega < 0$. This rotation can be broken down into two components. If we keep the generator angle $\gamma_+(s)$ the same as we rotate $\hat{g}_+$ from s to $s+ds$, the generator rotates due to the curvature of the crease line. This rotation is how much the curve tangent rotates in the material, given by the geodesic curvature $\kappa_g(s)\,ds$. Then if we rotate $\hat{g}_+$ at $s+ds$ to its new generator angle $\gamma_+(s+ds)$, the generator rotates due to the generator angle changing along the curve, given by $d\gamma_+(s) = \gamma'_+(s)\,ds$. The sum of these will be the total rotation of the generator $d\omega$, so we must have $\kappa_g(s) + \gamma'_+(s) < 0$. A similar argument can be carried out for generators in the outer surface, leading to $\kappa_g(s) - \gamma'_-(s) > 0$. These two inequalities can be written together as

$$\gamma'_\pm(s) < \mp\kappa_g(s), \tag{4.1}$$

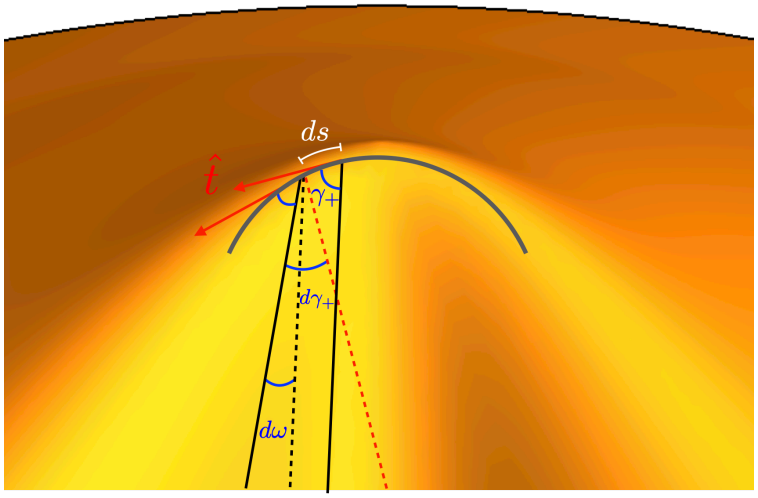

Figure 4.1: Rotation of an inner surface generator as one moves along the crease line. As one moves along the crease line (gray curved line), a material generator (solid black lines) will rotate in space, measured by the angle $d\omega$ between the original generator (dotted black line) and its neighbor. This rotation can be decomposed into two parts. If one transports the original generator along the crease while keeping the generator angle γ_+ the same, the generator rotates due to the curvature of the crease and aligns with the red dotted line. This line then rotates in order to line up with the neighboring generator, which comes from the generator angle changing along the crease. The angle of this rotation is therefore $d\gamma_+$.

and gives us a constraint at each point along the crease line that prohibits neighboring generators from intersecting. A similar inequality is presented in [38] for creased ribbons, and agrees with ours in the limit as the ribbon width goes to infinity. We will refer to this inequality throughout as the "positive splay condition."

Up until now we have considered creases in which the crease curve spans the entirety of the material surface. However, it is possible for the crease curve to have a length smaller than the size of the sheet, such as the crescent observed in the core of a d-cone, so that it is localized to a small region, and therefore must terminate within the material. This termination must occur in such a way so that the surrounding surface remains smooth and continuous. We will now discuss the conditions that enforce this.

We consider a termination point on the crease at a location denoted by s_t, and look at how the previously discussed quantities must behave at this termination point. As one

approaches s_t, the generators on either side must become more and more parallel so that the two surfaces of the crease meet at a common generator to form a continuous surface. This means that generator angles must be equal and opposite at the termination point: $\gamma_+(s_t) = -\gamma_-(s_t)$. However, these generator angles cannot be negative, as that would lead to the generators crossing from one side of the crease to the other. Therefore, we must have $\gamma_\pm(s_t) = 0$. Geometrically this means that the common generator at s_t must be parallel to the curve tangent. Furthermore, as one crosses this common generator, the surface normal must be continuous. This will be true if as we approach s_t, the tangent planes of each side become more parallel and the opening angle becomes larger and larger, so that $\theta(s_t) = \pi$.

We can say more about the behavior of τ and θ' at s_t by using the positive splay condition. We first expand our developability constraint, Eq. (3.12), near s_t:

$$\gamma_\pm \to \frac{\kappa_g \cdot (\theta - \pi)}{2(\tau \pm \theta'/2)}. \tag{4.2}$$

If the leading order behaviors of τ and θ near s_t are $\tau(s) \sim A\,(s - s_t)^\alpha$ and $\theta(s) \sim B\,(s - s_t)^{\beta+1} + \pi$ (so that $\theta'(s) \sim (\beta+1)B\,(s - s_t)^\beta$), we see that

$$\gamma_\pm(s) \sim \frac{\kappa_g(s_t) \cdot B\,(s - s_t)^{\beta+1}}{2(A\,(s - s_t)^\alpha \pm (\beta+1)B\,(s - s_t)^\beta/2)}. \tag{4.3}$$

If we then differentiate and normalize by $\kappa_g(s_t)$, we find

$$\Gamma'_\pm(s) \sim \frac{(\beta+1)B^2(s - s_t)^{2\beta} \mp 2AB(\alpha - \beta - 1)(s - s_t)^{\alpha+\beta}}{(2A\,(s - s_t)^\alpha \pm (\beta+1)B(s - s_t)^\beta)^2}, \tag{4.4}$$

where $\Gamma'_\pm \equiv \gamma'_\pm/\kappa_g$. We note that the possibility $\beta > \alpha$ is ruled out, as it entails that $\Gamma'_\pm \to 0$, and thus violates the positive splay condition of Eq. (4.1) on the inner surface, which requires $\Gamma'_+ < -1$ everywhere. Furthermore, when $\beta < \alpha$, $\Gamma'_\pm(s) \sim 1/(\beta+1)$, which also does not satisfy the positive splay condition, since β is non-negative. Therefore, in order to avoid intersecting generators near s_t, we must have $\beta = \alpha$. In other words, the ratio of

τ/θ' must approach a constant C as one approaches s_t. The value of C will be constrained by the positive splay condition, and will depend on the exact behavior of θ and τ near s_t, as we will see in Section 4.1.1. We can then summarize the conditions necessary for a continuous surface at s_t:

$$\gamma_\pm \to 0 \tag{4.5}$$

$$\theta \to \pi \tag{4.6}$$

$$\tau/\theta' \to C. \tag{4.7}$$

We note that Eq. (3.12) implies that the first constraint will be automatically satisfied if the second constraint is true, so in general only Eqs. (4.6) and (4.7) need to be satisfied.

It is reasonable, though not necessary, to also require that the surface of the crease is smooth everywhere. This means the mean curvature will be continuous everywhere, particularly at the joining generator. At s_t, Eq. (3.13) is indeterminate due to our earlier conditions, as $\kappa_{N\pm}(s_t)$ is zero while $\csc\gamma_\pm(s_t)$ is infinite. This indeterminacy can be resolved by expressing $H_\pm$ in terms of τ and θ' using Eq. (3.12). If we then expand the result around s_t, we get

$$H_\pm(s_t, v) \to \mp\frac{\tau(s_t) \pm \theta'(s_t)/2}{2(\gamma_\pm(s_t) \mp v(\kappa_g(s_t) \pm \gamma'_\pm(s_t))}. \tag{4.8}$$

We can impose the continuity condition at $s = s_t$. However, as mentioned at the end of Section 3.3, the mean curvature of the outer surface is positive while the mean curvature of the inner surface is negative. Therefore, in order for $H_\pm$ to be continuous along the line at which the two sides meet, the mean curvature must be zero at s_t. Assuming κ_g is finite at the termination point, this will be true if both τ and θ' vanish at s_t:

$$\theta' \to 0 \tag{4.9}$$

$$\tau \to 0. \tag{4.10}$$

4.1.1 Consequences

Even under the non-essential assumptions of nonvanishing κ_g and continuous mean curvature H, the termination conditions of Eqs. (4.5-4.7) and (4.9-4.10) impose only weak restrictions on the crease parameters θ and τ. Here we verify that these termination conditions are generally sufficient to give concrete realizations of surfaces with terminating creases. In order to see some of the consequences of having a terminating crease, let us assume the simplest scalings one can have for θ and τ that obey the above conditions, by doing an expansion about the termination point s_t for the generic case where $\kappa_g(s_t) \neq 0$:

$$\theta(s) = \pi + \Theta'' \, (\Delta\tilde{s})^2/2 + \mathcal{O}((\Delta\tilde{s})^4) \tag{4.11}$$

$$\tau(s) = C \, \Theta'' \, \kappa_g(s_t)\Delta\tilde{s} + \mathcal{O}((\Delta\tilde{s})^3) \tag{4.12}$$

where $\Theta'' \equiv \theta''(s_t)/\kappa_g^2(s_t)$ and $\Delta\tilde{s} \equiv \kappa_g(s_t) \cdot (s - s_t)$. In order to find $\gamma_\pm(s)$ around s_t, we can substitute the above scalings into Eq. (4.2):

$$\gamma_\pm(s) \approx \frac{1}{2(2C \pm 1)}\Delta\tilde{s} + \mathcal{O}((\Delta\tilde{s})^3). \tag{4.13}$$

As mentioned in Section 4.1, the values C can take are constrained by the positive splay condition. We can see this by differentiating the above and using the positive splay condition:

$$\frac{1}{2(2C \pm 1)} < \mp 1. \tag{4.14}$$

We first consider the more restrictive requirement on the inner surface, corresponding to the upper signs. In order for this inequality to be satisfied on the inner surface, the left hand side must be negative, so that $C < -1/2$. Furthermore, we can rearrange the inequality to get $C > -3/4$, so that C is bounded both below and above: $-3/4 < C < -1/2$. Note that this automatically satisfies Eq. (4.14) on the outer surface.

We finally would like to see how much elastic bending energy is stored in a sector of the

crease near the termination point. If we substitute in our scaling relations into Eq. (3.16), using the approximations $\sec^2\gamma_\pm \approx 1$ and $\sin\gamma_\pm \approx \gamma_\pm$ we get

$$dE = \frac{B}{8}\,d\tilde{s}\sum_{\pm}\pm\left[\frac{(2C\pm 1)^3\Theta''^2(\Delta\tilde{s})^2}{2(4C\pm 3)}\log\left(\frac{\Delta\tilde{s}\mp R\kappa_g(4C\pm 3)}{\Delta\tilde{s}}\right)+\mathcal{O}((\Delta\tilde{s})^3)\right]. \quad (4.15)$$

4.2 Finite symmetric crease

So far we have considered the behavior of a crease near a termination point in the material. However, in order to know the energy cost needed to form the crease, we must consider its global behavior. Since the d-cone core crescent is symmetric, we will consider symmetric creases which have two termination points. We choose $s = 0$ to be the symmetry point, so that the termination points are at $\pm s_t$. In addition to conditions at the termination points, there are also conditions τ, θ', and $\gamma_\pm$ must satisfy at the symmetry point. By symmetry, $\tau(s)$ and $\theta'(s)$ must be odd functions, and therefore must be zero at $s = 0$. The generator at $s = 0$ also has to be perpendicular to the crease, so that $\gamma_\pm(0) = \pi/2$, which is actually automatically true by Eq. (3.12). Finally, we must satisfy the positive splay condition. As seen in Section 4.1.1, we may expand Eq. (3.12) (this time around $s = 0$), differentiate with respect to s, and write the result in non-dimensional form:

$$\Gamma'_\pm(0) \approx \frac{\tau'(0)\pm\theta''(0)/2}{\kappa_g^2(0)\cot\theta_0/2} \quad (4.16)$$

where θ_0 is the opening angle at $s = 0$. This must obey $\Gamma'_\pm < \mp 1$.

CHAPTER 5

EXAMPLES

5.1 Crease with constant geodesic curvature

We now demonstrate a range of realizable surfaces, using several strategies. We consider specific examples of finite symmetric creases, which obey the conditions outlined in Chapter 4. The first example we consider is a crease formed from a circular arc, i.e. a crease with constant geodesic curvature. As explained in Section 3.3, the crease shape will be fully determined if one specifies κ_g, τ, and θ everywhere along the crease. We choose the simplest functional forms for θ and τ such that they obey all of the conditions outlined previously:

$$\theta(s) = (\theta_0 - \pi)\bar{s}^2(\bar{s}^2 - 2) + \theta_0 \tag{5.1}$$

$$\tau(s) = C\theta'(s) = \frac{4\phi}{s_t}\bar{s}(\bar{s} - 1)(\bar{s} + 1) \tag{5.2}$$

where $\bar{s} \equiv s/s_t$ and $\phi \equiv C(\theta_0 - \pi)$ is the total twist of the crease line from the center to the tip. We can find constraints on ϕ, θ_0, and s_t from the positive splay condition. At s_t, the result follows from Eq. (4.14), and puts limits on the value of ϕ: $(\pi - \theta_0)/2 < \phi < 3(\pi - \theta_0)/4$. Further constraints can be found by applying the positive splay condition at the symmetry point $s = 0$, as discussed in Section 4.2. Furthermore, we have found that if the positive splay condition is satisfied both at the symmetry point and at the termination points, it will be satisfied everywhere along the crease. An example of this type of crease is shown in Fig. 5.1a.

5.2 Crease with cylinder on one side

As explained earlier in Section 3.3, the crease shape can also be determined by specifying one surface and the geodesic curvature of the crease. Here we treat the simple case where the inner surface lies on a cylinder. The cylinder case is of particular interest, since it only

marginally satisfies the positive splay condition. This surface is obtained by wrapping a flat sheet, and so is developable by construction. We again choose our crease curve to have a constant geodesic curvature, and so the curve's shape is fully determined by κ_g and the radius of the cylinder L. We take the axis of our cylinder to be along the z-direction, and parametrize our curve as follows:

$$\vec{X}(s) = \left(L\cos\left(\frac{\sin\kappa_g s}{\kappa_g L}\right), L\sin\left(\frac{\sin\kappa_g s}{\kappa_g L}\right), (1/\kappa_g)\cos\kappa_g s \right) \tag{5.3}$$

One readily verifies that $\vec{X}'(s)$ is of unit length and is tangent to the surface of the cylinder at $\vec{X}(s)$. Furthermore the curvature vector $\vec{X}''(s)$ has a component in the tangent plane of the cylinder at $\vec{X}(s)$ of magnitude κ_g. In order for our curve to satisfy the condition $\gamma_\pm \to 0$ as $s \to s_t$, the crease line's tangent $\vec{X}'(s)$ must point along the cylinder axis at $\pm s_t$. We must therefore have $\kappa_g s_t = \pi/2$ so that the curve spans a half-arc of a circle. Note that the generators on the inner surface are parallel by construction, so that they automatically satisfy the positive splay condition. The outer side of the crease will be determined as outlined in Section 3.3, so that we can specify our crease for any given κ_g and L. An example of such a crease is shown in Fig. 5.1b.

We note that at the termination points, our crease does not satisfy the zero mean curvature condition, due to the fact that the cylindrical side has a constant non-zero curvature everywhere. As argued in Section 4.1, this means that the mean curvature must be discontinuous at the tip. Such discontinuities are common in physical sheets, as when a sheet is peeled away from a flat, adhesive substrate [45]. This discontinuity does not prevent the construction of continuous, isostatic deformation around the crease. It leads us to study sheets with such discontinuities more generally. Therefore, we may consider other examples where there is a jump in the mean curvature at the termination points.

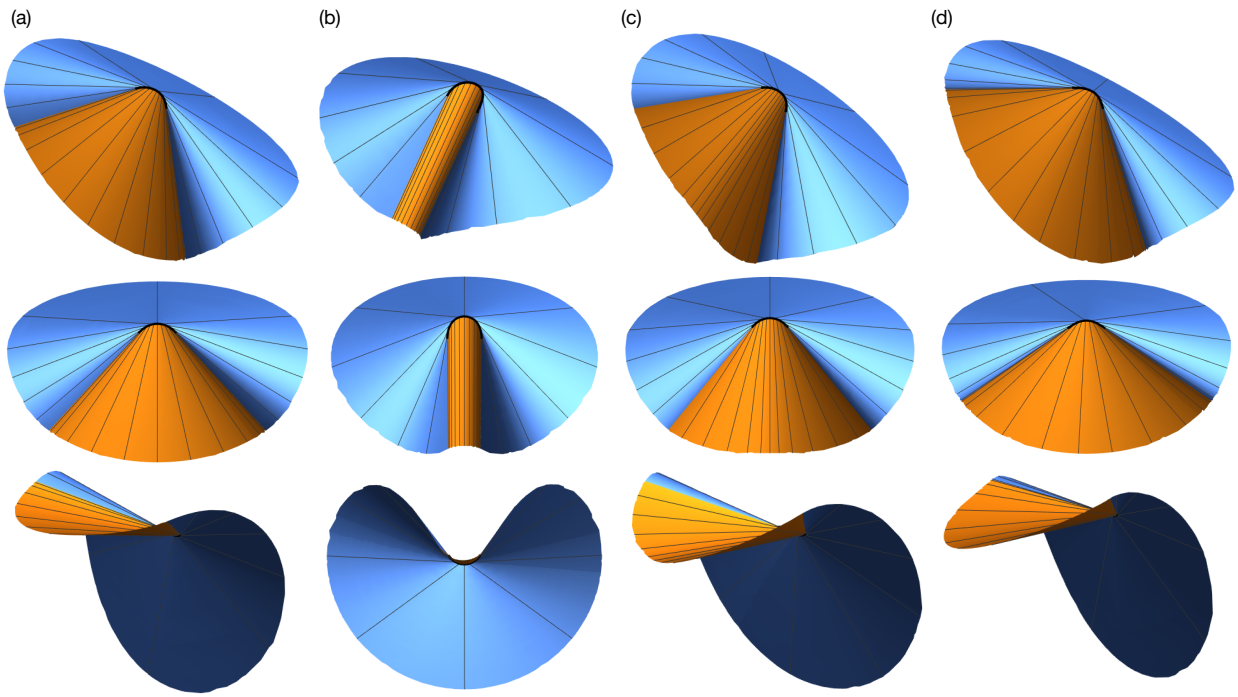

Figure 5.1: Examples of finite curved creases. Curved bold lines indicate the crease line, orange and blue surfaces correspond to the inner and outer surfaces respectively, and thin straight lines indicate the generators. Each row corresponds to a different viewpoint of the crease, with the first row being an off-angle view, the second a view along the symmetry line of the crease, and the third a view along the generator at which the two sides of the crease meet. (a) Crease with zero mean curvature at termination points, with $\kappa_g = 1$, $\theta_0 = \pi/2$, $s_t = \pi/4$, and $\phi = 3\pi/8$. (b) Crease with a cylinder as the inner surface, with $\kappa_g = 1$ and $L = 1$. (c) Crease with mean curvature jump at termination points, with $\kappa_g = 1$, $\theta_0 = \pi/2$, $s_t = \pi/4$, and $\phi = 3\pi/8$. (d) Crease with a vanishing geodesic curvature at termination points, with $\kappa_g(s) = -(s^2 - s_t^2)$, $\theta_0 = \pi/2$, $s_t = \pi/4$, and $\phi = 3\pi/8$.

5.3 Constant geodesic curvature crease with mean curvature discontinuity

If we relax the zero mean curvature condition at the termination points, the continuous mean curvature conditions given by Eqs. (4.9) and (4.10) are no longer required. Thus we no longer need τ and θ' to vanish at s_t. We can then choose simpler expressions for θ and τ such that they only vanish at the symmetry point:

$$\theta(s) = (\pi - \theta_0)\bar{s}^2 + \theta_0 \tag{5.4}$$

$$\tau(s) = C\theta'(s) = -\frac{2\phi}{s_t}\bar{s} \tag{5.5}$$

where again $\bar{s} \equiv s/s_t$ and $\phi \equiv C(\theta_0 - \pi)$ is the total twist of the crease line from the center to the tip. Similar to the crease described in Section 5.1, ϕ will have bounds due to the positive splay condition, this time being $(\pi - \theta_0)/2 < \phi < (\pi - \theta_0)$. We show an example of this type of crease in Fig. 5.1c.

5.4 Crease with vanishing geodesic curvature

So far we have only considered cases where the geodesic curvature was constant, but we also can have a varying geodesic curvature and still satisfy our conditions at the termination points. One interesting case is when κ_g vanishes at s_t, so that the crease line straightens as we approach the termination points. This will affect our termination conditions, as we shall now see.

The mean curvature near s_t has the same form as before, given by Eq. (4.8). However, we now must take into account what happens when κ_g vanishes at s_t. Let us assume τ is a constant at s_t, and that θ and κ have the leading order behaviors $(s - s_t) + \pi$ and $(s - s_t)^\alpha$ respectively (so θ' is constant at s_t as well). From Eq. (4.2), we see that $\gamma_\pm(s) \sim (s - s_t)^{\alpha+1}$, so that $\gamma'_\pm(s) \sim (s - s_t)^\alpha$. If we substitute these scalings into Eq. (4.8), we find that the

denominator vanishes while the numerator does not, so that the mean curvature diverges at the termination point. In order to avoid this divergence, we must have the numerator of Eq. (4.8) vanish in such a way that $H_{\pm}(s_t, v)$ is constant. Therefore, both τ and θ' must vanish at s_t, as they did when we required H to be smooth. How fast exactly they vanish is important, as we will now see.

For simplicity, we now assume that τ and θ have the same leading order behavior near s_t, i.e. $\tau(s) \sim \theta'(s) \sim (s - s_t)^{\beta}$, so that the numerator of Eq. (4.8) has this same behavior. Assuming κ_g near s_t has the same behavior as above, we can substitute these new scalings into Eq. (4.2) to find $\gamma_{\pm}(s) \sim (s - s_t)^{\alpha+1}$. Differentiating this leads to $\gamma'_{\pm}(s) \sim (s - s_t)^{\alpha}$, so that $\gamma'_{\pm}$ has the same scaling as κ_g. Since $\gamma_{\pm}(s)$ vanishes at s_t faster than $\gamma'_{\pm}(s)$ (and therefore $\kappa_g(s)$), we can ignore it in the denominator of Eq. (4.8), so that the denominator goes as $(s - s_t)^{\alpha}$. Therefore, in order to have $H_{\pm}(s_t, v)$ be a nonzero constant, we must have $\alpha = \beta$. In other words, τ and θ' must vanish just as fast as κ_g at the termination points. This will result in a jump in the mean curvature, since as mentioned before, the mean curvature of the inner and outer surfaces are of opposite sign. Furthermore, if we have $\alpha < \beta$, so that the numerator of Eq. (4.8) vanishes faster than the denominator, then the mean curvature will vanish at s_t, and so will be continuous from one side of the crease to the other. This actually is a generalization of our zero mean curvature condition for the non-vanishing geodesic curvature case: τ and θ' must vanish faster than κ_g, whether κ_g vanishes or not at s_t. We show an example of this particular crease with vanishing geodesic curvature in Fig. 5.1d, using the same functional forms for τ and θ as in Section 5.1.

CHAPTER 6

CREASE ENERGETICS

As noted above, the final shape of the creased surface can be altered by external forcing; our conditions of isometry are not sufficient to determine the shape. The actual shape with given forcing is that of minimal bending energy. In this chapter we investigate how the crease parameters affect this energy.

In order to examine the bending energy resulting from curved creases, we turn back to our first example of a constant geodesic curvature crease described in Section 5.1. This crease is described by three parameters: θ_0, s_t, and ϕ. If we compare to the d-cone, θ_0 is related to the d-cone deflection, and so is a parameter we can control. Then for a given θ_0, we can find values of s_t and ϕ which minimize the total bending energy (found by integrating Eq. (3.16) from one end of the crease to the other), subject to the constraint imposed by the positive splay condition. An example heatmap of the bending energy is shown in Fig. 6.1.

However, the bending energy also depends on the size of the sheet. This means that the optimal values of s_t and ϕ may in general depend on our chosen size of the sheet. Since we are considering asymptotically large sheets, we want to be able to minimize the energy independently of R. In the large R limit, the bending energy is given by

$$E \approx \frac{B}{8} \sum_{\pm} \mp \int ds \frac{(\tau \pm \theta'/2)^2 \sec^2 \gamma_\pm}{\kappa_g \pm \gamma'_\pm} \log \left(\mp \frac{R(\kappa_g \pm \gamma'_\pm)}{\sin \gamma_\pm} \right), \tag{6.1}$$

which clearly has a logarithmic dependence on R on each side of the crease. We can separate out this logarithmic dependence by rewriting the integrand above in the form $a_\pm(s) \cdot \log(R/d_\pm(s))$, where

$$a_\pm(s) \equiv \mp \frac{(\tau \pm \theta'/2)^2 \sec^2 \gamma_\pm}{8(\kappa_g \pm \gamma'_\pm)} \tag{6.2}$$

and $d_\pm(s)$ is the local cone vertex distance defined in Section 3.3. We then separate

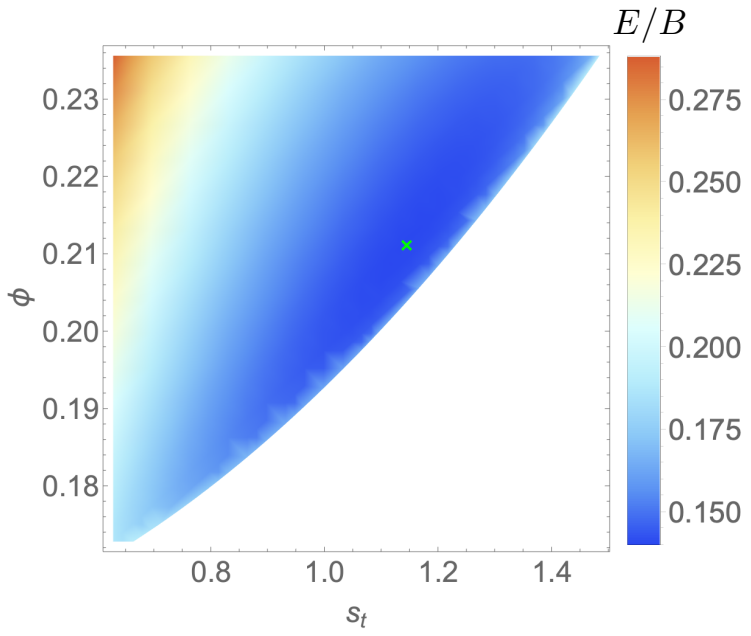

Figure 6.1: Heatmap of energy for a finite size crease with $\kappa_g = 1$, $R = 10$, and $\theta_0 = 0.9\pi$. Cooler colors indicate a smaller energy, with the minimum indicated by a light green cross. The blank region in the lower right hand part of the plot indicates the region where the positive splay condition on the inner surface is no longer satisfied.

the logarithm into two terms and integrate each of them separately over the extent of the crease, resulting in $E \approx B \sum_{\pm} A_{\pm}(\log R - D_{\pm}/A_{\pm})$, where $A_{\pm} \equiv \int a_{\pm}(s)\, ds$ and $D_{\pm} \equiv \int a_{\pm}(s) \log d_{\pm}(s)\, ds$. Finally, defining $\log r_{\pm} \equiv D_{\pm}/A_{\pm}$ and combining the logarithms, we get

$$E \approx B \sum_{\pm} A_{\pm} \log \frac{R}{r_{\pm}} \tag{6.3}$$

Since R is large, the logarithm dominates the prefactor in the expression, which has no R dependence. If we remove the logarithmic dependence from Eq. (6.3), we can instead minimize the sum of the prefactors $A_{\pm}$ in order to find the equilibrium shape of a crease in the large R limit. An example heatmap of the integrated prefactor is shown in Fig. 6.2a. We can therefore find values of s_t and ϕ that minimize $A_{\pm}$ extrapolated to infinite R for several chosen values of θ_0, as shown by the blue circles in Fig. 6.2b, and see that as the crease angle becomes more pronounced, the preferred crease length becomes shorter and the crease twists more out of plane (this is visually more obvious in the shapes shown in Fig. 6.2c).

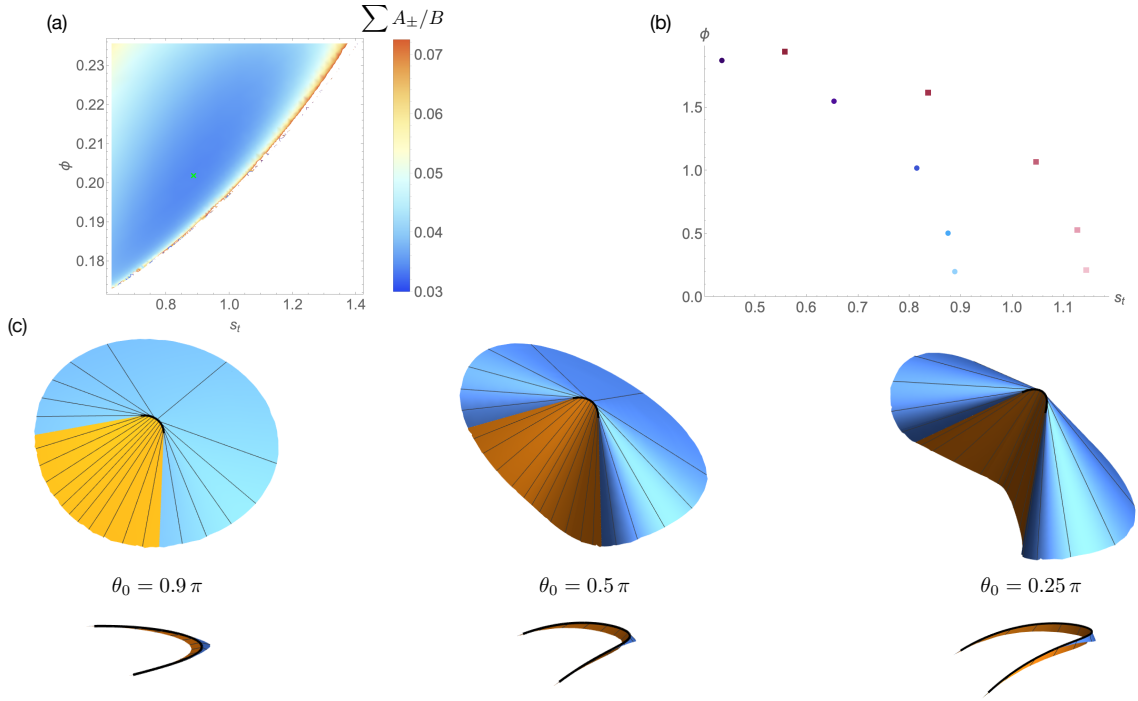

Figure 6.2: (a) Heatmap of $A_\pm$ for crease with $\kappa_g = 1$ and $\theta_0 = 0.9\pi$. Cooler colors indicate a smaller prefactor, with the minimum indicated by a light green cross. The blank region in the lower right hand part of the plot indicates the region where the positive splay condition on the inner surface is no longer satisfied. (b) Parameter values which minimize the bending energy. The red squares are the values which minimize the the energy for a finite size sheet with $R = 10$, while the blue circles correspond to the values which minimize $A_\pm$. Values of θ_0 used are $0.1\,\pi$, $0.25\,\pi$, $0.5\,\pi$, $0.75\,\pi$, and $0.9\,\pi$, and lighter colored points correspond to larger values of θ_0. (c) Equilibrium shapes of finite creases for different θ_0. Bottom row shows the shape of the crease, which becomes more twisted as θ_0 gets smaller.

This increasing twist is also observed in other known creases, such as the narrow circular creases in [38], where the crease buckles out of plane as one folds along the mid-line. These trends are also observed when minimizing the energy of finite-size sheets, as shown by the red squares in Fig. 6.2b.

We can also compare the energies of the different examples constructed in Chapter 5. For this comparison, we use the shapes shown in Fig. 5.1, whose parameters were chosen so that they had similar opening angles, crease lengths, and twist. We find that the energies of the shapes a, c, d are nearly the same, with the energy of the outer surface being around an order of magnitude larger than the inner energy. The remaining shape, whose inner surface

is a cylinder, however exhibits a very different behavior. While we chose a cylinder radius so that the opening angle and twist angle were comparable to those of the other examples, the crease length will be fixed for a given κ_g, as explained in Section 5.2. Furthermore, because the inner surface is a cylinder, its bending energy will not depend logarithmically on R, but instead linearly, so that the inner energy dominates for large sheets.

We have said in Section 3.1 that a finite curved crease can potentially describe the crescent observed in the d-cone core, but we have not yet justified why this proves to be better than previous approaches. In order to do so, we will compare it to the traditional picture of the d-cone. As described in Section 2.2, the traditional picture treats the outer and core regions separately, where the outside is an isometric cone whose generators have a common intersection point, and the core is a region of stress focusing whose size R_c is set by a balance between bending and stretching. The total (bending) energy of the outer cone region is given by Eq. (2.3), and exhibits a logarithmic dependence on the sheet size R. As we noted above, in the large R limit, the bending energy of a curved crease has a logarithmic dependence on R as well, in the form $E \approx B \sum_{\pm} \int ds\, a_{\pm}(s) \cdot \log(R/d_{\pm}(s))$. This is not surprising, since as explained in Section 4.1, locally each segment of the crease is part of a cone. In fact, if we compare this expression to Eq. (2.3), we see that at each point s along the crease there is an effective R_c, which is the distance from the crease to the local cone vertex $d_{\pm}(s)$, and is non-zero everywhere along the crease except at the two termination points. The vanishing of $d_{\pm}(s)$ at the termination points does lead to divergences of the energy density at these points, but these divergences are in general integrable, so that the total energy of the crease will be finite. Additionally, as we showed above, one can fully separate out the R dependence in the energy, leading to Eq. (6.3), which shows that each side of the crease has a global effective R_c, given by $r_{\pm}$. In the traditional approach, one excludes the d-cone core region when calculating the bending energy of the overall structure to avoid a divergence at the tip. However, for the crease, in the zero-thickness limit, its bending energy will be finite without having to exclude any region around the crease line. This suggests that viewing the d-cone

as a finite curved crease is more advantageous than previous approaches, as it can describe the d-cone core crescent along with the entire surrounding material with just its bending energy, without imposing a cutoff near the crescent.

CHAPTER 7

DISCUSSION

We have outlined conditions necessary to have a finite curved in an unstretchable sheet, and constructed several examples of such structures. However, in order to fully justify that a curved crease can accurately describe the global structure of a d-cone, there are some features of curved creases that should be cross-checked with observable features of a real d-cone. We have also only considered unstretchable sheets so far and have not discussed creases in finite-thickness materials. Furthermore, we have not directly addressed how our approach may help understand the observed scaling of the d-cone core radius, and how it might reconcile with the energy balance arguments put forth so far to determine the core radius.

Since our crescents successfully produce the qualitative shape of a d-cone, and since we expect the d-cone shape to come to a fixed limit asymptotically, the crease model seems to be a good way to get testable predictions about this shape. Certain qualitative tests already appear feasible. First, as described in Section 3.3, the binormal vector of the crease line $\hat{b}$ will be parallel to the line bisecting the opening angle of the crease. This means the normal vector of the crease line $\hat{n}$ must be perpendicular to this bisector. If one measures the shape profile of the d-cone core crescent, $\hat{n}$ can be determined everywhere along the crescent. One can then measure the opening angle profile, determine its bisector along the crease, and compare it to $\hat{n}$. A second test involves the curvatures of the surfaces on either side. One can measure the mean curvature profile of the surface, particularly at the symmetry line of the crescent, where the generators will be orthogonal to the crescent. At the crescent itself, the mean curvature will be just half the normal curvature κ_N. Then combined with the opening angle θ and the crescent curvature κ at the symmetry point, one can verify whether the compatibility condition of Eq. (3.9b), i.e. $\kappa_{N\pm} = \pm\kappa\cos\theta/2$, holds on both sides. A similar analysis could also be done at any point in the surface by comparing to the expected mean curvature given by Eq. (3.13), though one would also have to know the

generators in the surface. A third observation involves the tip of the crescent. Our analysis shows that the mean curvature of a crease with a non-negative κ_g cannot change sign except at the termination point, and the generators must be parallel to the tangent vector there. This implies that the crescent line points along the inflection line of a d-cone. Finally, the curvature $\kappa(s)$ and torsion $\tau(s)$ of the crescent can be determined from the measured crescent profile, as well the opening angle $\theta(s)$. Our construction would then be able to infer the outer shape and compare it with the expected circular outer shape of a real d-cone.

We have so far only talked about the energy cost due to bending of the sheet around the crease. If there were no external forces involved, such as from folding along the crease line or confining the sheet, the equilibrium shape of the material would just be a flat sheet. When the crease forms, the surrounding material bends and acquires elastic energy, but the formation of the crease itself in the material must cost some amount of energy as well. One can account for this, for instance, by assigning the crease a stiffness and an equilibrium angle at which the crease's energy cost is minimized, as done by [38]. Additionally, in real sheets the thickness is no longer zero, and there will be stretching in addition to bending, which will be localized around the crease. There are two known cases which account for stretching near a line singularity in a thin sheet. The first is the stretching ridge described in Section 2.1. However, a stretching ridge is always straight, and so cannot account for the curvature of the crease line. The other case is known as the ring ridge, which appears when one deforms a spherical shell until a dent forms [46]. In the formation of this ridge, the ring will radially move inward, resulting in a compressive strain along the circle that is linear in the ridge width. This differs from the stretching ridge, where the strain is due to a transverse displacement of the ridge line, and so is quadratic in the ridge width. While the curved crease does not exactly map to the ring ridge, in the nearly-flat case, a curved crease will be a finite arc of a circle, in which case a similar analysis can be applied.

If we consider a curved crease as a segment of a ring ridge whose width is w, the induced strain γ will be proportional to $\kappa_g w$. Since the area is proportional to $s_t w$, the stretching

energy is of order $E_s \sim (B/h^2)\gamma^2 s_t w \sim B\kappa_g^2 w^3 s_t/h^2$. There is also a bending energy due to the ridge width, which is of order $E_b \sim Bw^{-2} s_t w \sim Bs_t/w$. Minimizing the sum of these two yields an optimal ridge width of $w \sim (h/\kappa_g)^{1/2}$, similar to that of a ring ridge. Extending this analysis to a non-flat crease is not straightforward, since as one decreases the opening angle, the crease line's curvature is no longer constant and its torsion is no longer zero. This is demonstrated in Fig. 6.2b, as we see that the twist of the crease is comparable to the angular extent of the crease. Therefore, we do not treat the general case here.

In Chapter 6, we discussed the subtlety of minimizing the bending energy in the asymptotically large R limit, as the equilibrium shape of a crease will in general depend on the sheet size. It would seem the same should be true for a d-cone. Experiments and simulations are limited in the sheet thickness-to-size ratios they are able to probe, and so cannot explore the asymptotically large R limit. While others have consistently observed the core size scaling $R_c \sim h^{1/3}R^{2/3}$, this may not be the true scaling for asymptotically large sheets. Therefore, it is possible that if previous studies were carried out with a much larger dynamic of thickness-to-size ratios, one would observe a core size is proportional to the thickness, which would be consistent with energy balance arguments.

Finally, we would like make some comparisons between our curved crease structures and d-cones. We have shown several examples of terminating creases in Fig. 5.1, which all have crease lines similar to the observed core crescent. However, the outer behavior is clearly different: the outer surfaces are not conical, but instead flatten out towards the symmetry line of the crease. This is to be expected, since we do not implement any constraints to support the other side like in a d-cone, but instead constrain the shape of the crease line. One could enforce the outer surface to be a cone geometrically, but one must be careful about the liftoff region, as this occurs on the outer surface, so the entire outer surface of the crease cannot be a cone. One could also adjust the functional forms for κ_g, τ, and θ in order to adjust the curvature of outer surface while still satisfying the termination conditions. However, we are still forced to acknowledge that the crease picture is incomplete, in terms

of determining the length of the crease line. While we are able to find equilibrium shapes of curved creases, the finite thickness of the sheet is never considered, and so we cannot expect to learn about the dependence of the crescent length on the thickness without something additional.

CHAPTER 8

CONCLUSION

We believe our approach of treating the d-cone core crescent as a curved crease may give new insight into understanding the energetics of the core region. One does not have to separate the core region from the outer conical region as previous approaches do. This seems more promising to understanding why the core radius could have any dependence on the outer dimensions of the sheet. Furthermore, there are other similar structures that may be studied by this approach. An example is the Pogorelov ring ridge: when one deforms the dimple more and more, at some point it is energetically favorable for the ring to buckle, forming a polygonal ridge with straight ridges meeting at sharp corners. These corners have similarities to the d-cone core crescent. Another example are the forced vertices studied by Gottesman et al [35]. These are formed in a way similar to that of a d-cone, but may exhibit different core radii based on the forcing protocol. By examining the exact geometry of the crescent via curved creases, we hope the observed scaling of R_c can be properly reconciled.

REFERENCES

[1] Alexander E. Lobkovsky. *Structure of crumpled thin elastic membranes*. PhD thesis, The University of Chicago, 1996.

[2] Andrea Cavagna, Alessio Cimarelli, Irene Giardina, Giorgio Parisi, Raffaele Santagati, Fabio Stefanini, and Massimiliano Viale. Scale-free correlations in starling flocks. *Proceedings of the National Academy of Sciences*, 107(26):11865–11870, 2010.

[3] Malcolm J. Andrews and Stuart B. Dalziel. Small atwood number rayleigh-taylor experiments. *Philosophical Transactions of the Royal Society A: Mathematical, Physical and Engineering Sciences*, 368(1916):1663–1679, 2010.

[4] L.P. Kadanoff. *Statistical Physics: Statics, Dynamics and Renormalization*. Statistical Physics: Statics, Dynamics and Renormalization. World Scientific, 2000.

[5] JM Lehn. Supramolecular chemistry-concepts and chemistry. *VCH: Wiley: Weinheim*, 1995.

[6] M. Wyart and M. E. Cates. Discontinuous shear thickening without inertia in dense non-brownian suspensions. *Phys. Rev. Lett.*, 112:098302, Mar 2014.

[7] Peter Goldreich and Scott Tremaine. The formation of the cassini division in saturn's rings. *Icarus*, 34(2):240 – 253, 1978.

[8] Edward N. Lorenz. Deterministic nonperiodic flow. *Journal of the Atmospheric Sciences*, 20(2):130–141, 10/12/2020 1963.

[9] Jesse Berezovsky. The structure of musical harmony as an ordered phase of sound: A statistical mechanics approach to music theory. *Science Advances*, 5(5), 2019.

[10] Raymond E. Goldstein and Alain Goriely. Dynamic buckling of morphoelastic filaments. *Phys. Rev. E*, 74:010901, Jul 2006.

[11] Fan Xu, Chenbo Fu, and Yifan Yang. Water affects morphogenesis of growing aquatic plant leaves. *Phys. Rev. Lett.*, 124:038003, Jan 2020.

[12] Natalie K. Gordon and Richard Gordon. The organelle of differentiation in embryos: the cell state splitter. *Theoretical Biology and Medical Modelling*, 13(1):11, 2016.

[13] R Graham Park. *Foundation of structural geology*. Routledge, 2013.

[14] M Considère. *Mémoire sur l'emploi du fer et de l'acier dans les constructions*. Vue Ch. Dunod, 1885.

[15] Eran Sharon, Benoît Roman, Michael Marder, Gyu-Seung Shin, and Harry L. Swinney. Buckling cascades in free sheets. *Nature*, 419(6907):579–579, 2002.

[16] John Nash. C1 isometric imbeddings. *Annals of Mathematics*, 60(3):383–396, 1954.

[17] Leonhard Euler. *Methodus inveniendi lineas curvas maximi minimive proprietate gaudentes*. apud Marcum-Michaelem Bousquet, 1744.

[18] Julien Chopin and Arshad Kudrolli. Helicoids, wrinkles, and loops in twisted ribbons. *Phys. Rev. Lett.*, 111:174302, Oct 2013.

[19] Hunter King, Robert D. Schroll, Benny Davidovitch, and Narayanan Menon. Elastic sheet on a liquid drop reveals wrinkling and crumpling as distinct symmetry-breaking instabilities. *Proceedings of the National Academy of Sciences*, 109(25):9716–9720, 2012.

[20] Jesse L. Silverberg, Arthur A. Evans, Lauren McLeod, Ryan C. Hayward, Thomas Hull, Christian D. Santangelo, and Itai Cohen. Using origami design principles to fold reprogrammable mechanical metamaterials. *Science*, 345(6197):647–650, 2014.

[21] Ludwig Prandtl. Über flussigkeitsbewegung bei sehr kleiner reibung. *Verhandl. III, Internat. Math.-Kong., Heidelberg, Teubner, Leipzig, 1904*, pages 484–491, 1904.

[22] C. Upstill and John Frederick Nye. Light caustics from rippling water. *Proceedings of the Royal Society of London. A. Mathematical and Physical Sciences*, 365(1720):95–104, 1979.

[23] M. Ben Amar and Y. Pomeau. Crumpled paper. *Proceedings of the Royal Society of London. Series A: Mathematical, Physical and Engineering Sciences*, 453(1959):729–755, 1997.

[24] T. A. Witten. Stress focusing in elastic sheets. *Rev. Mod. Phys.*, 79:643–675, Apr 2007.

[25] Omer Gottesman, Jovana Andrejevic, Chris H. Rycroft, and Shmuel M. Rubinstein. A state variable for crumpled thin sheets. *Communications Physics*, 1(1):70, 2018.

[26] B. Audoly and Y. Pomeau. *Elasticity and Geometry: From hair curls to the non-linear response of shells*. OUP Oxford, 2010.

[27] M.P. do Carmo. *Differential Geometry of Curves and Surfaces*. Prentice-Hall, 1976.

[28] Alexander E. Lobkovsky and T. A. Witten. Properties of ridges in elastic membranes. *Phys. Rev. E*, 55:1577–1589, Feb 1997.

[29] E. Cerda and L. Mahadevan. Conical surfaces and crescent singularities in crumpled sheets. *Phys. Rev. Lett.*, 80:2358–2361, Mar 1998.

[30] E. Cerda and L. Mahadevan. Confined developable elastic surfaces: cylinders, cones and the elastica. *Proceedings of the Royal Society A: Mathematical, Physical and Engineering Sciences*, 461(2055):671–700, 2005.

[31] Sahraoui Chaïeb and Francisco Melo. Crescent singularities and stress focusing in a buckled thin sheet: Mechanics of developable cones. *Phys. Rev. E*, 60:6091–6103, Nov 1999.

[32] Tao Liang and Thomas A. Witten. Crescent singularities in crumpled sheets. *Phys. Rev. E*, 71:016612, Jan 2005.

[33] Jin W. Wang. Rim curvature anomaly in thin conical sheets revisited. *Phys. Rev. E*, 84:066603, Dec 2011.

[34] T Mora and A Boudaoud. Thin elastic plates: On the core of developable cones. *Europhysics Letters*, 59(1):41–47, jul 2002.

[35] Omer Gottesman, Efi Efrati, and Shmuel M. Rubinstein. Furrows in the wake of propagating d-cones. *Nature Communications*, 6(1):7232, 2015.

[36] Huffman. Curvature and creases: A primer on paper. *IEEE Transactions on Computers*, C-25(10):1010–1019, Oct 1976.

[37] J. P. Duncan and J. L. Duncan. Folded developables. *Proceedings of the Royal Society of London. A. Mathematical and Physical Sciences*, 383(1784):191–205, 1982.

[38] Marcelo A. Dias, Levi H. Dudte, L. Mahadevan, and Christian D. Santangelo. Geometric mechanics of curved crease origami. *Phys. Rev. Lett.*, 109:114301, Sep 2012.

[39] Marcelo A. Dias and Basile Audoly. A non-linear rod model for folded elastic strips. *Journal of the Mechanics and Physics of Solids*, 62:57 – 80, 2014.

[40] Marcelo A. Dias and Christian D. Santangelo. The shape and mechanics of curved-fold origami structures. *Europhysics Letters*, 100(5):54005, dec 2012.

[41] Martin Kilian, Simon Flöry, Zhonggui Chen, Niloy J. Mitra, Alla Sheffer, and Helmut Pottmann. Curved folding. In *ACM SIGGRAPH 2008 Papers*, SIGGRAPH '08, New York, NY, USA, 2008. Association for Computing Machinery.

[42] S.M. Farmer and C.R. Calladine. Geometry of "developable cones". *International Journal of Mechanical Sciences*, 47(4):509 – 520, 2005.

[43] Keith A. Seffen. Spherical images and inextensible curved folding. *Phys. Rev. E*, 97:023004, Feb 2018.

[44] M. Spivak. *A Comprehensive Introduction to Differential Geometry Vol. 3*. Publish or Perish, Incorporated, 1975.

[45] Q. D. Yang, M. D. Thouless, and S. M. Ward. Analysis of the symmetrical 90 °-peel test with extensive plastic deformation. *The Journal of Adhesion*, 72(2):115–132, 2000.

[46] A.V. Pogorelov. *Bendings of Surfaces and Stability of Shells*. American Mathematical Society, 1988.